Numerical Experiments on Lee Cyclogenesis

JOSEPH EGGER

Institut für Theoretische Meteorologie der Universität München, 8 München 2, Federal Republic of Germany

(Manuscript received 3 August 1973; in revised form 2 July 1974)

ABSTRACT

Cyclogenesis in the lee of long north-sourth barriers is studied by use of a numerical weather prediction model. Lee-side development is simulated by the model if an initial situation is chosen, which is favorable for lee cyclogenesis, i.e., a low approaching the barrier from the west in a baroclinic current. Cyclogenesis is investigated in the lee of a barrier of 4000 km length and 2000 m height, which is comparable to the Rocky Mountains, and of another one, which is similar to the massif of Greenland. In both cases, the divergence equation and the vorticity equation are analyzed at the point of greatest pressure fall in the lee to find out the causes of the lee-side development.

Pressure fall begins when the parent low approaches the barrier. It is caused by the warm air that is crossing the barrier in front of the approaching center of low pressure. Vorticity advection aloft is of no importance in the Rocky Mountains case and influences the surface pressure only during the final period of pressure fall in the Greenland case. The development is terminated when the cold front of the parent low passes over the new center of low pressure in the lee. An attempt is made to compare the predictions of the model to observations in the lee of the Rocky Mountains and of Greenland.

1. Introduction

Large mountain barriers, such as the Rocky Mountains or the Andes Mountains, exert a pronounced influence on the atmospheric flow at all scales. In the synoptic scale, vortices are generated in the lee of mountain ranges. For evidence one may refer to the charts of frequency of cyclogenesis by Klein (1957), which show distinct maxima of cyclogenesis in the lee of the Rocky Mountains, near Greenland, in the Gulf of Genoa, etc. In recent years, much effort has been devoted to studies of cases of lee cyclogenesis. For example, Hage (1961) tried to assess the role of vorticity advection aloft during cyclogenesis in Alberta; Newton (1956) stressed the influence of horizontal differences of friction in generating vorticity. Walden (1959) described the situations which are favorable for cyclogenesis on the east coast of Greenland.

In spite of these efforts, no satisfactory explanation of lee cyclogenesis has been presented so far. This is not surprising in view of the complexity of the problem. A theory that aims at an explanation of lee cyclogenesis has to take into account the essential features of the synoptic patterns near the mountains which are favorable for the lee cyclogenesis—it should contain a realistic description of orography and should be able to deal with nonlinear processes. Furthermore, the networks of sounding stations in cyclogenetic regions are not dense enough to make feasible a satisfactory check of any theory of observations.

Another way to deal with lee cyclogenesis is to simulate it in numerical models. It is possible to predict lee cyclogenesis by use of a numerical weather prediction (NWP) model starting from a realistic initial situation (e.g., Egger, 1972a). A careful analysis of the output of the model should result in an improved understanding of the mechanism of lee cyclogenesis in the model. Then, conclusions may be drawn on the causes of lee cyclogenesis in nature, provided that the predicted patterns are close enough to the observed ones. The method of analysis used in this paper is similar to that employed by the author in numerical experiments on cyclogenesis in the Gulf of Genoa (Egger, 1972b). It consists of an investigation of the divergence equation and of the vorticity equation at grid points of the cyclogenetic region. Experiments have been made with a very long barrier (4000 km) and one of 2400 km length in order to simulate cyclogenesis in the lee of the Rocky Mountains (Section 4) and of Greenland (Section 5).

2. The model

Our NWP model is very similar to that described by Edelmann (1963). It is a σ-model which is based on the primitive equations (σ=pressure/surface pressure). It has five layers in the vertical (Fig. 3) and a staggered grid is used with a horizontal grid length of 350 km. The β-plane approximation is applied. The model includes a very simple parametrization of surface

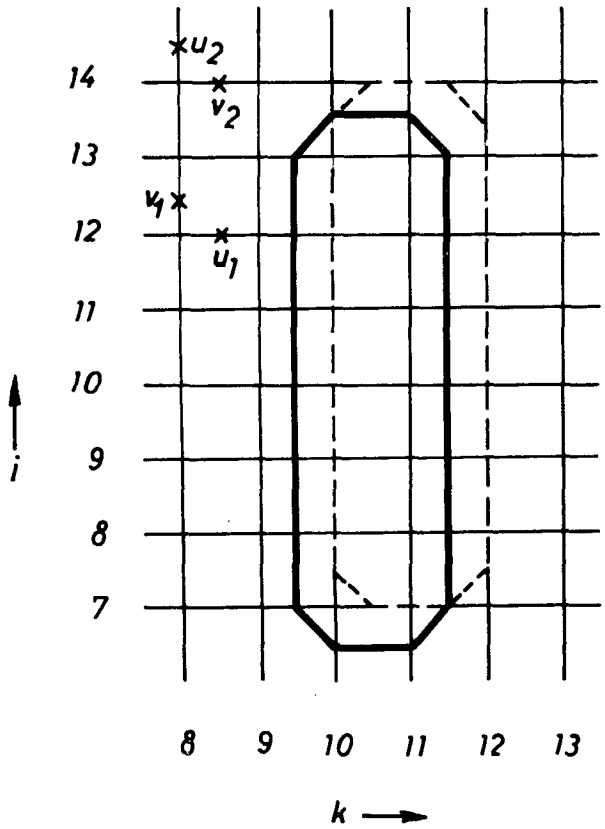

FIG. 1. Contour of the "Greenland-barrier" at odd time steps (solid) and at even time steps (dashed) in the grid of the model. The components of the horizontal wind are defined at different positions at odd (subscript 1) and even (subscript 2) time steps; k (i) is the index of the grid points in x (y) direction.

friction and horizontal diffusion, but no moisture, no heat flux from the ground, and no radiation processes.

The integration domain is a channel with a cyclic boundary condition on the eastern and western boundaries and a rigid wall at the northern and southern boundaries. An orographic barrier is placed in the channel.

Figure 1 shows the contours of the mountain barrier in the grid of the model which has been used in the Greenland case. The coast line of Greenland is represented in the model by the heavy solid line in Fig. 1. An enormous wall rises from sea level to a height of about 2000 m along the coast line of Greenland. In order to estimate this rapid ascent a vertical wall of about 2000 m height is erected along this line in the model. The modeling of this wall is done by putting

$$v_n=0 \tag{1}$$

in all grid points of the contour line in the lowest level $\sigma=0.9$, where v_n is the component of the wind normal to the wall. The lowest layer of the model has a thickness of about 2000 m ($1.0\geq\sigma\geq 0.8$). Furthermore, we impose $u=v=0$ at all grid points inside the barrier. Thus, the mountain is represented as a mass of stagnant air. Accordingly, the surface pressure inside the vertical walls is evaluated at sea level and not at the top of the mountain. Figure 3 shows an east-west cross section of the barrier. The ice dome of Greenland is not represented. Hence, the top of the mountain coincides almost with the coordinate surface $\sigma=0.8$.

It should be noted that there is a shift of the position of the wall between even and odd time steps (Fig. 1), which is accomplished in order to overcome a tendency towards a separation of the predictions at even and odd time steps. The reader is referred to a paper of the author (Egger, 1972a) for a more detailed description and discussion of the modeling of such a wall.

3. The tendency of divergence and vorticity

The tendency of the surface pressure is given by

$$\frac{\partial\pi}{\partial t}=-\int_0^1 \nabla\cdot(\pi\mathbf{V})d\sigma, \tag{2}$$

where $\mathbf{V}=(u;\,v)$ is the wind in the surfaces of constant σ and π is the dimensionless surface pressure. Lee cyclogenesis is initiated and maintained if the atmospheric flow is mainly divergent ($\nabla\cdot(\pi\mathbf{V})>0$) in the lee of the barrier during a numerical experiment. Therefore, a discussion of the causes of cyclogenesis can be based on an examination of the course of $\nabla\cdot(\pi\mathbf{V})$ in the levels above the area of the greatest pressure fall in the lee, which is determined by the divergence equation

$$\frac{\partial}{\partial t}\nabla\cdot(\pi\mathbf{V})=\underbrace{-\left[\frac{\partial^2}{\partial x^2}(\pi uu)+2\frac{\partial}{\partial x\partial y}(\pi uv)+\frac{\partial^2}{\partial y^2}(\pi vv)\right]}_{\text{DHA}}$$

$$-\left[\frac{\partial}{\partial\sigma}\nabla\cdot(\pi\mathbf{V}\dot{\sigma})\right]+\underbrace{\left[f\left(\frac{\partial}{\partial x}(\pi v)-\frac{\partial}{\partial y}(\pi u)\right)-\beta\pi u\right]}_{\text{CVORT}}$$

$$-[\nabla\cdot(\pi\nabla\Phi)]-[\nabla\cdot(RT\nabla\pi)], \tag{3}$$

which is deduced from (2) and the equations of horizontal motion

$$\frac{\partial u}{\partial t}=-u\frac{\partial u}{\partial x}-v\frac{\partial u}{\partial y}-\dot{\sigma}\frac{\partial u}{\partial\sigma}+fv-\frac{\partial\Phi}{\partial x}-\frac{RT}{\pi}\frac{\partial\pi}{\partial x} \tag{4}$$

$$\frac{\partial v}{\partial t}=-u\frac{\partial v}{\partial x}-v\frac{\partial v}{\partial y}-\dot{\sigma}\frac{\partial v}{\partial\sigma}-fu-\frac{\partial\Phi}{\partial y}-\frac{RT}{\pi}\frac{\partial\pi}{\partial y} \tag{5}$$

(Coriolis parameter $f=f_0+\beta y$; Φ, geopotential; T, temperature; $\dot{\sigma}$, $=d\sigma/dt$).

During a numerical experiment, all terms of (3) in brackets are evaluated at each time step in the cyclogenetic area. The experiments show that the first term DHA—describing the influence of horizontal

advection—has no decisive effect on the pressure fall. The next one does not contribute to changes of π because of the boundary condition $\dot{\sigma}=0$ for $\sigma=0$, $\sigma=1$, i.e.,

$$\int_0^1 \frac{\partial}{\partial\sigma}\nabla\cdot(\pi\mathbf{V}\dot{\sigma})d\sigma=0. \tag{6}$$

CVORT mainly gives the influence of the relative vorticity on the development for $-\beta\pi u$ is of minor importance. Cyclonic vorticity is favorable for a growth of $\nabla\cdot(\pi\mathbf{V})$ and for pressure fall

In our experiments, the surface $\sigma=1$ coincides with sea level even in the mountain area. Thus, $|\nabla\pi|$ is not extremely large in the mountainous regions as is the case with usual σ-models. Then, an interpretation of the last two terms of (3) can be given by use of the approximations

$$-\nabla\cdot(\pi\nabla\Phi)\sim-\pi\int_\sigma^1 R\nabla^2T\frac{\partial\sigma}{\sigma}, \tag{7}$$

$$-\nabla\cdot(RT\nabla\pi)\sim-RT\nabla^2\pi. \tag{8}$$

The validity of these approximations has been verified in numerical experiments (Egger, 1972b). Hence, $-\nabla\cdot(\pi\nabla\Phi)$ at a certain level is mainly determined by the Laplacian of temperature in all layers below that level. One has to expect a cyclogenetic influence of (7) in a point with ∇^2T 0 in all layers, i.e., in a point with comparatively warm air. The term $-\nabla\cdot(RT\nabla\pi)$ is approximately proportional to the Laplacian of surface pressure; $\nabla^2\pi$ is positive in the center of a low.··· Thus, (8) gives the anticyclogenetic influence of the distribution of the surface pressure.

Pressure fall in the lee of the mountains can be brought about by an increase of vorticity or by a decrease of ∇^2T in most of the layers. The causes of a change of vorticity can be seen from the corticity equation

$$\frac{\partial\zeta}{\partial t}=-\mathbf{V}\cdot\nabla\zeta-\dot{\sigma}\frac{\partial\zeta}{\partial\sigma}-\zeta\nabla\cdot\mathbf{V}-\beta v-f\nabla\cdot\mathbf{V}+\frac{\partial\dot{\sigma}}{\partial y}\frac{\partial u}{\partial\sigma}-\frac{\partial\dot{\sigma}}{\partial x}\frac{\partial v}{\partial\sigma}$$
$$+\frac{\partial}{\partial y}\left(\frac{RT}{\pi}\frac{\partial\pi}{\partial x}\right)-\frac{\partial}{\partial x}\left(\frac{RT}{\pi}\frac{\partial\pi}{\partial y}\right) \tag{9}$$

where $\zeta=\partial v/\partial x-\partial u/\partial y$ is the relative vorticity in σ-surfaces. The horizontal advection and $(\zeta+f)\nabla\cdot\mathbf{V}$ contribute significantly to the tendency of vorticity in our case. All other terms are of minor importance.

Two cases of lee cyclogenesis will be investigated in detail. The first experiment is performed with a barrier of 4000 km length and the second with the Greenland barrier as shown in Fig. 1.

Eqs. (3) and (9) in finite difference form will be studied in the grid point of greatest pressure fall in the lee.

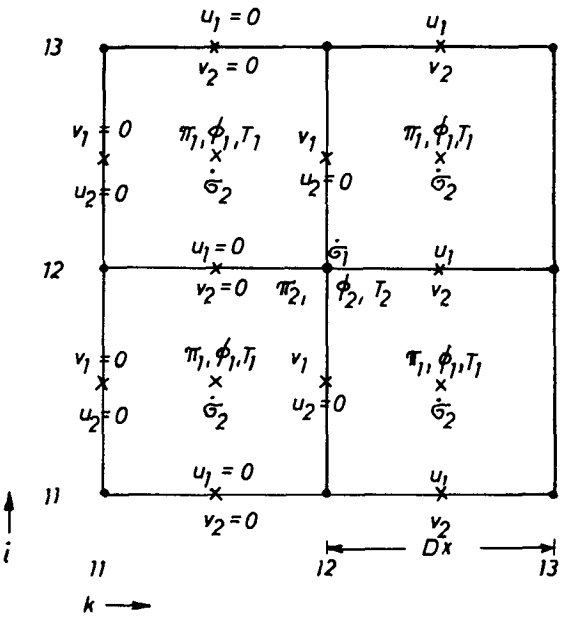

Fig. 2. The grid of the model near the point of the greatest pressure fall ($k=12$; $i=12$) and the boundary conditions of the mountain wall in the lowest layer. See text for further explanation.

Figure 2 shows the staggered grid of the model near the grid point ($k=12$; $i=12$) where k,i is the index of the grid points in the x,y directions, respectively. The point (12; 12) is close to the eastern wall of the barrier and is the point of maximum pressure fall in the first experiment (see Fig. 2; circle in Fig. 4). The quantities π, Φ, T are defined in the grid points at even time steps (subscript 2), u_2 in $(k;\ i+\frac{1}{2})$, v_2 in $(k+\frac{1}{2};\ i)$. The situation at odd time steps (subscript 1) may be seen from Fig. 2. The boundary condition (1) and the conditions inside the wall are satisfied near (12; 12) in the lowest level $\sigma=0.9$ by posing $u_2=0$ in all points with $k=12$ or $k=11$, $v_2=0$ in those with $k=11.5$, $u_1=0(v_1=0)$ in those with $k=11.5(k=11)$.

Using the conventional notation

$$u_x=(u_{k+\frac{1}{2}}-u_{k-\frac{1}{2}})/Dx$$

$$\bar{u}^x=(u_{k+\frac{1}{2}}+u_{k-\frac{1}{2}})/2,$$

etc., where Dx is the grid length, (4) and (5) are written in finite difference form

$$u_t=-\bar{u}^{xy-y}u_x-\bar{v}^{yy-x}u_y-\bar{\dot{\sigma}}^{y-xy}u_\sigma+fv-\Phi_x-\frac{\overline{RT}^x}{\bar{\pi}^x}\pi_x, \tag{10}$$

$$v_t=-\bar{u}^{xx-y}v_x-\bar{v}^{xy-x}v_y-\bar{\dot{\sigma}}^{x-xy}v_\sigma-fu-\Phi_y-\frac{\overline{RT}^y}{\bar{\pi}^y}\pi_y, \tag{11}$$

Then, the tendency of $\nabla\cdot(\pi\mathbf{V})$ in finite difference form

is given by

$$\frac{\partial}{\partial t}\nabla\cdot(\pi\mathbf{V})\approx[(\overline{u\pi}^{y})_x+(\overline{v\pi}^{x})_y]_l. \qquad (12)$$

In (12; 12), however, one has to be cautious in the lowest level because of the boundary condition

$$u=u_l=0$$

in the point (11.5; 12). Hence,

$$\frac{\partial}{\partial t}\nabla\cdot(\pi\mathbf{V})\approx[(\overline{u\pi}^{y})/Dx_{k=12.5,\ i=12}+(\overline{v\pi}^{x})_y]_l$$

in the lowest level instead of (12). Therefore, the terms of the right-hand side of (10) in the point (11.5; 12) do not contribute to the finite difference form of (3) in the lowest level. For example, $\nabla\cdot(RT\nabla\pi)$ is not approximated by

$$\nabla\cdot(RT\nabla\pi)\approx R(\overline{T}^{x}\pi_x)_x+R(\overline{T}^{y}\pi_y)_y$$

but by

$$\nabla\cdot(RT\nabla\pi)_c\approx R(\overline{T}^{x}\pi_x)/Dx_{k=12.5,\ i=12}+R(\overline{T}^{y}\pi_y)_y.$$

The subscript c will be used for terms which have to be corrected because of the boundary conditions at the mountain wall.

All terms of (3) and (9) have been computed in all levels. A simplification of the discussion can be attained by adding up these terms for the two uppermost levels ($\sigma=0.1$, $\sigma=0.3$) and for the middle levels ($\sigma=0.5$; $\sigma=0.7$). The subscript l is introduced to characterize the terms of (3) and (9) in the level $\sigma=0.9$, which is below the crest height of the barrier, whereas the subscripts m and u mark the sums of these terms in the middle and upper layer (Fig. 3).

4. Barrier of 4000 km length—Rocky Mountains

The studies of Hess and Wagner (1948), Newton (1956), Hage (1961) and others reveal clearly that

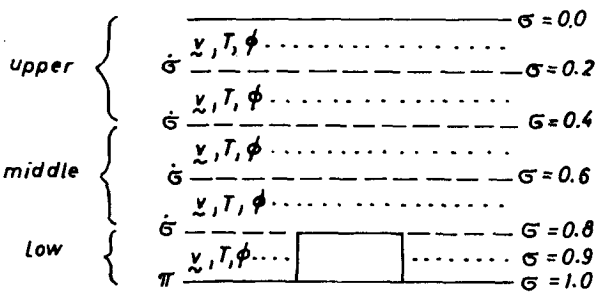

FIG. 3. East-west cross section of the mountain barrier and the vertical structure of the model.

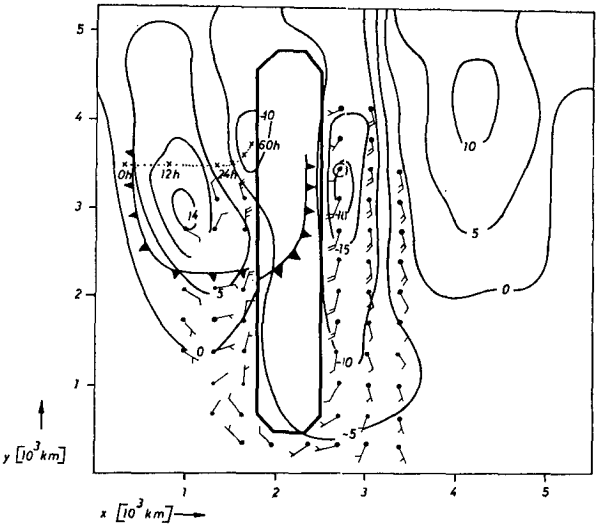

FIG. 4. Long barrier. Deviation of the surface pressure (mb) from the initial basic state after 60 hr. Wind in $\sigma=0.9$ (odd time steps). The grid point (12; 12) is encircled. Track of the low's center (dots).

cyclogenesis in the lee of the Rocky Mountains is initiated in most cases by a migratory low from the Pacific. The new cyclone on the eastern slope is being formed, while the upper level trough is crossing the mountains.

The most satisfactory way to study such cases of cyclogenesis in a numerical model would have been to make 2–3 day hemispheric forecasts starting, say, at the day before the new cyclone has been observed. However, the forecast domain of our model is a channel. Then, it is not possible to make satisfactory forecasts with real data beyond, say, one day since the time dependent boundary conditions for the channel are not known. Instead, we prescribe an initial state which simulates the synoptic situation favorable for lee cyclogenesis, i.e., a low west of the barrier drifting in a baroclinic current towards the mountain range. In our experiments, this "basic" zonal current $\bar{u}$ has no horizontal shear but a uniform vertical shear of 4 m/s (100 mb). We chose $\bar{u}=0$ in $\sigma=0.9$ ($\bar{u}=-2$ m/s in $\sigma=1.0$). Hence, the mountain barrier does not block the basic current since the boundary conditions (1) are satisfied in the level $\sigma=0.9$.

A low with a diameter of 1800 km is superposed on this basic flow about 1500 km west of the barrier which has a maximum vorticity of 0.5 10^{-4} s^{-1} in its center in all levels. Initially, the wind field in the channel is in geostrophic balance. We have, therefore, a south-north gradient of the surface pressure in order to balance the easterly zonal wind at the surface. The barrier in the model depicts only the main features of the Rocky Mountains. We use a simple barrier of 4200 km length, 1000 km width, and 2000 m height as shown in Fig. 4 instead of the complicated topographic pattern of the Rocky Mountains.

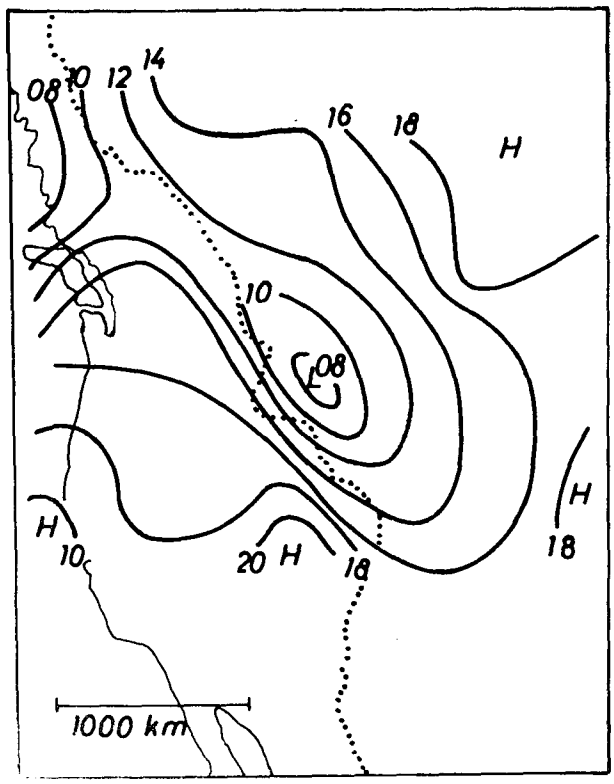

FIG. 5. Mean sea-level isobars, when an average lee-side cyclocone has reached its greatest intensity. After Hess and Wagner (1948).

Figure 4 shows the deviation of the surface pressure from the initial basic state after 60 hr. The low moved straight towards the barrier during the first 24 hr (dots). Then, deceleration and a curving towards the north can be seen together with a filling of the surface low. The outbreak of cold air in the rear of the low is indicated by the "cold front" which has been drawn at the points of maximum horizontal pressure gradient in the level $\sigma=0.9$ (in $\sigma=0.7$ above the barrier). After one day, the surface pressure begins to fall in the lee of the barrier and a long narrow region of low pressure can be noted after 60 hr. A ridge has been established in front of a broad zone of southerly flow east of the mountain range.

Hess and Wagner (1948) compiled charts of a mean life history of the lee cyclones in the Montana region by averaging the maps of 10 similar cases of lee cyclogenesis at various stages of development. Figure 5 shows the mean sea-level isobars when the lee cyclone has reached its greatest intensity and is about to become migratory. This stage of development corresponds closely to that displayed in Fig. 4, for there is no pressure fall after $t=60$ hr, and the new cyclone begins to move southeastward in the experiment. The area of the most intense pressure fall is restricted to a narrow tongue in the lee just as in Fig. 4 (see also Fig. 20 by Bonner, 1961; Fig. 21 by McClain, 1960). The surface low on the western slope, which moved in from the Pacific, is filling very rapidly. The ridges over the Great Basin and over Saskatchewan can be seen even 36 hr before the lee cyclone reaches its greatest intensity. Thus, the model's inability to simulate the Great Basin high might be due to the oversimplified initial situation of our experiment. The cyclone formation in Fig. 4 occurred ahead of the cold front of the Pacific cyclone in good agreement with observations (see Fig. 15 by Newton, 1956; Bonner, 1961, p. 7).

Figure 6 shows the deviation of the height of the 500-mb surface from the basic state after 60 hr. The center of the parent cyclone decelerated while approaching the mountains and is curving towards the south above the western wall (compare with Fig. 6 of Hage, 1961). The influence of the new cyclone reaches up to 500 mb, as observed in many cases. On the other hand, the amplitudes of the waves in Fig. 6 are rather weak in comparison to real cases of cyclogenesis. This deficiency is partly caused by our choice of a zonal basic current at the beginning of our experiment. Usually, a pronounced longwave pattern is observed at the beginning of the lee cyclogenesis in the Rockies. A ridge over the mountains is followed by a deep cold trough over the Pacific surface low. The upper trough is moving inland at a much faster rate than in our case and overtakes the new surface center, say, one day after the beginning of the pressure fall. Nevertheless, the main features of typical cases of lee cyclogenesis have been simulated fairly realistically by the model. Therefore, one should be able to obtain some insight into the mechanism of the lee cyclogenesis by analyzing the numerical experiment. To that end, (3) and (9) are studied in the grid point (12; 12).

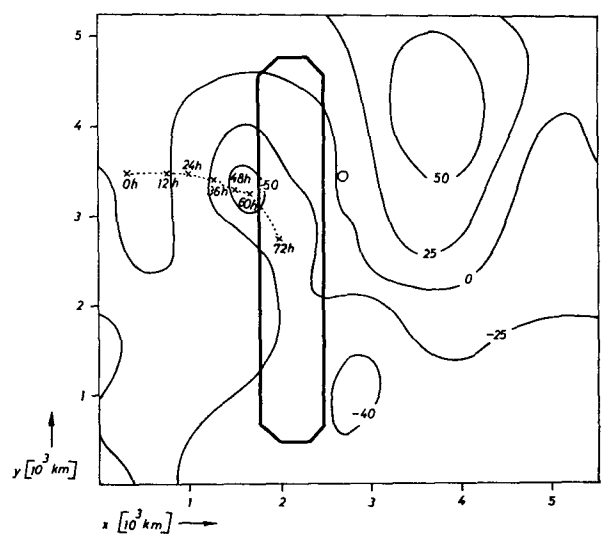

FIG. 6. Long barrier. Deviation of the height (m) of the 500-mb surface from the basic initial state after 60 hr. Dots: the track of the center of the low at 500 mb. Circle: grid point (12; 12).

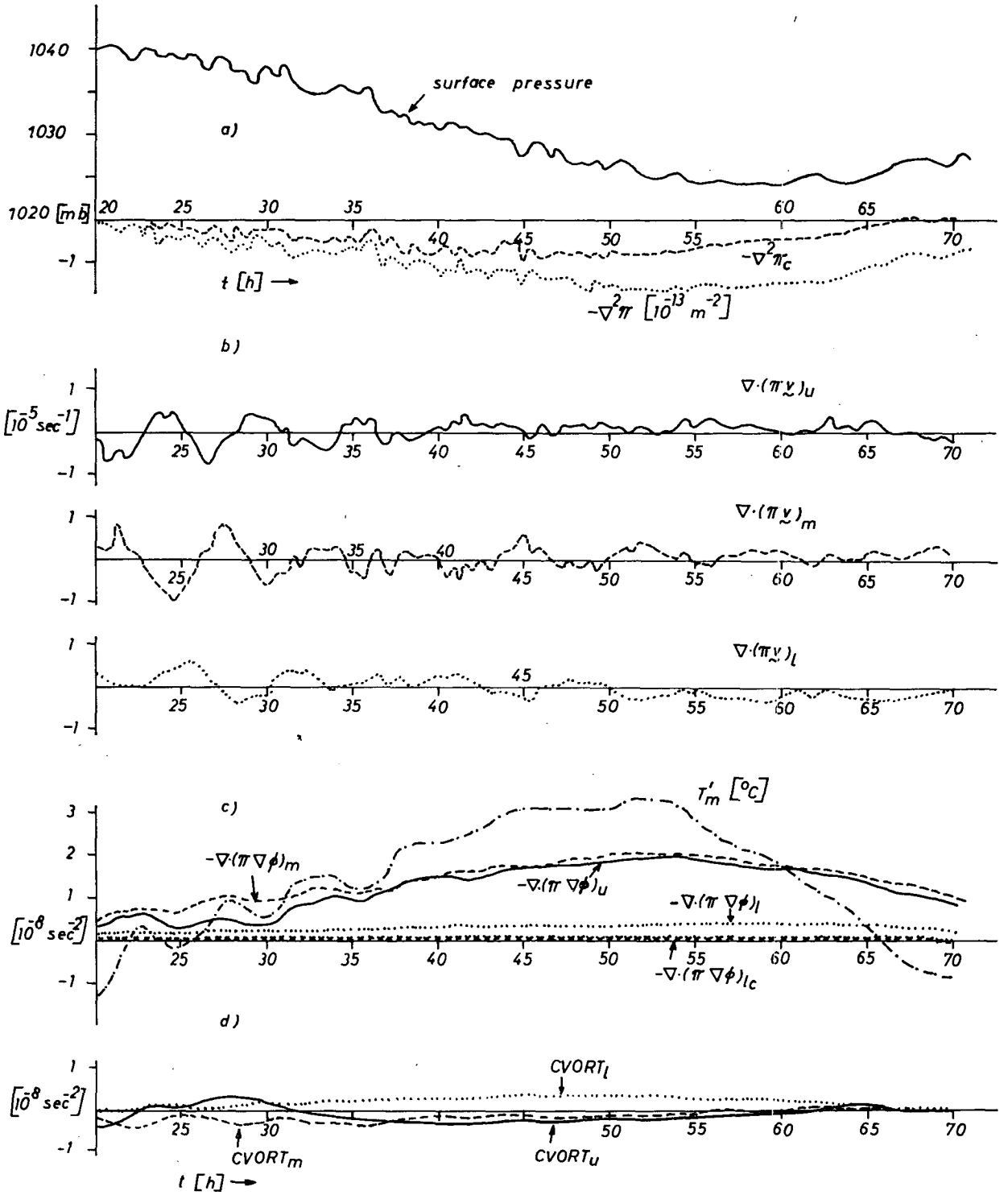

FIG. 7. Long barrier $20 \leq t \leq 70$ hr. Grid point (12; 12). (a) Surface pressure (mb); $-\nabla^2\pi$ (dots) and the corrected form $-\nabla^2\pi_c$ which takes into account the influence of the barrier in the lowest layer (dashed). (b) $\nabla\cdot(\pi\mathbf{V})$ in all three layers. (c) Deviation T_m' of T_m from the initial temperature distribution. $-\nabla\cdot(\pi\nabla\Phi)$ in all layers and the corrected form $-\nabla\cdot(\pi\nabla\Phi)_{lc}$. (d) CVORT in all layers.

Figure 7(a) shows the surface pressure in (12; 12) from $t=20$ hr until $t=70$ hr. The pressure fall begins at about 25 hr and is going on with many short interruptions until about 60 hr. The total pressure fall amounts to 16 mb. The pressure is rising later on.

The quantity $-\nabla^2\pi$ (dots) is negative all the time and reaches its minimum at about the same time as the surface pressure. Thus, $-\nabla\cdot(RT\nabla\pi)$ aims at a decrease of $\nabla\cdot(\pi\mathbf{V})$ in the middle and upper layer. The corrected value $-\nabla^2\pi_c$, which should be used in the lowest level, is negative, too, but always larger than $-\nabla^2\pi$. The barrier reduces the anticyclonic influence of the surface pressure distribution.

The quantity $\nabla\cdot(\pi\mathbf{V})$ in the three layers is shown in Fig. 7(b). Strong oscillations prevail until about 35 hr. There is mainly weak divergence ($\nabla\cdot(\pi\mathbf{V})>0$) in the upper layer from $t=40$ hr until 65 hr. The middle layer is essentially divergent after $t=44$ hr, whereas the lowest layer undergoes a change from a divergent regime towards a convergent one ($\nabla\cdot(\pi\mathbf{V})<0$) at about 50 hr. Accordingly, there is mainly downward motion until 50 hr and upward motion later on in the lowest level. Descent on the slopes during low-level development has been reported by Newton (1956), McClain (1960), and Bonner (1961), and has often been quoted to explain the increase of vorticity during cyclogenesis by stretching.

We have pressure fall if $\nabla\cdot(\pi\mathbf{V})_{l+m+u}>0$. The pressure fall from 31 hr until 33 hr, for example, is obviously caused by the increase of $\nabla\cdot(\pi\mathbf{V})_l(\nabla\cdot(\pi\mathbf{V})_m)$ from 30 hr (28 hr) until 34 hr (32.5 hr). A decrease of $\nabla\cdot(\pi\mathbf{V})_u$ is counteracting. Such changes of $\nabla\cdot(\pi\mathbf{V})$ are induced by changes of the terms of (3). The term $-\nabla\cdot(RT\nabla\pi)$ can be inferred from Fig. 7(a) according to (8). This term is negative in all layers and exerts an anticyclonic influence. The term $-\nabla\cdot(\pi\nabla\Phi)$ is shown in Fig. 7(c). The value of $-\nabla\cdot(\pi\nabla\Phi)$ is almost the same in the middle and upper layers. Thus, the influence of the temperature distribution in the upper layer on $-\nabla\cdot(\pi\nabla\Phi)_u$ is negligible, as shown in (7). The term $-\nabla\cdot(\pi\nabla\Phi)_m$ is increasing steadily from $t=20$ hr until 55 hr, and is decreasing later on. Therefore, the temperature field has a cyclogenetic influence in our case. The term $-\nabla\cdot(\pi\nabla\Phi)_l$ is positive, too, but very small. The corrected value $-\nabla\cdot(\pi\nabla\Phi)_{lc}$ is even smaller. The temperature distribution seems to have no significant influence on the cyclogenetic process in the lowest layer.

An inspection of Fig. 7(d) shows that there is weak anticyclonic vorticity in the middle and upper layer nearly all the time, and an increase of cyclonic vorticity from 25 hr until about 50 hr in the lowest level. The maximum vorticity of 0.5 10^{-4} s^{-1}, which is attained at about 50 hr, is rather weak.

There is southerly flow east of the barrier from 20 hr until the end of development (Fig. 4). Southerly flow along the eastern slopes is often observed during the first stages of the development in the lee of the Rockies (see Fig. 18 by Newton (1956); Figs. 2–3 by Bonner (1961); Fig. 4 by Carlson, 1961), but northerly flow is seen near the slopes after the new cyclone has gained enough strength to establish its own circulation. Our low with its comparatively weak development did not reach this state until $t=72$ hr.

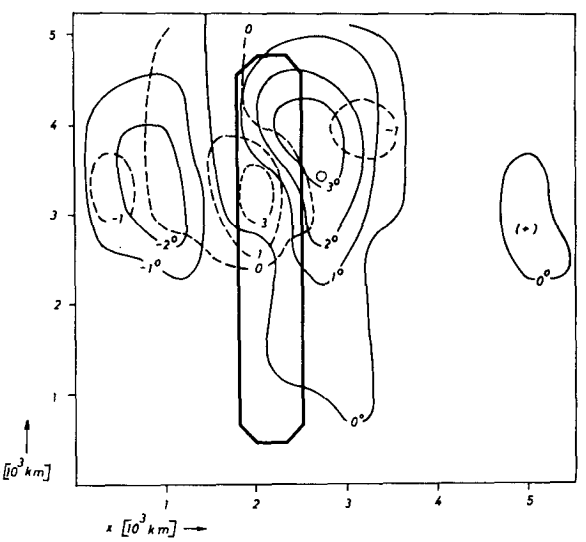

FIG. 8. Long barrier. Vorticity (10^{-5} s^{-1}; dashed) and the deviation of the temperature from the basic initial state in $\sigma=0.7$ after 48 hr.

An examination of the term DHA in (3) shows that DHA is less than 10^{-9} s^{-2} all the time. The oscillations of $\nabla\cdot(\pi\mathbf{V})$ during the period $20<t<35$ hr are influenced by DHA, but the trend of $\nabla\cdot(\pi\mathbf{V})$ is not influenced by DHA.

It can be stated that the pressure fall at the point (12; 12) is initiated and maintained by $-\nabla\cdot(\pi\nabla\Phi)$. The vorticity plays a weak anticyclogenetic role in the middle and upper layer and contributes towards pressure fall in the lowest layer; $-\nabla\cdot(RT\nabla\pi)$ is always negative and anticyclogenetic.

Thus, our case differs from the Pettersen hypothesis (in which orography is not considered) that cyclone development at sea level occurs when and where an area of appreciable vorticity advection aloft becomes superimposed upon a low-level frontal system or a baroclinic zone. It has been shown by Hage (1961) that this rule is valid in many cases of lee cyclogenesis. A growth of $\mathrm{CVORT}_{u,m}$ in (3) may lead to an increase of $\nabla\cdot(\pi\mathbf{V})_{u,m}$ and pressure fall under favorable conditions. However, the studies of Newton (1956), Bonner (1961), and Hage (1961; case 38-2) make it clear that positive vorticity advection aloft is not a necessary condition for the lee cyclogenesis.

How can we explain the increase of $-\nabla\cdot(\pi\nabla\Phi)$ in the middle layer? A rise of $-\nabla\cdot(\pi\nabla\Phi)_m$ has to be effected by a decrease of ∇^2T, i.e., by an increase of the tempera-

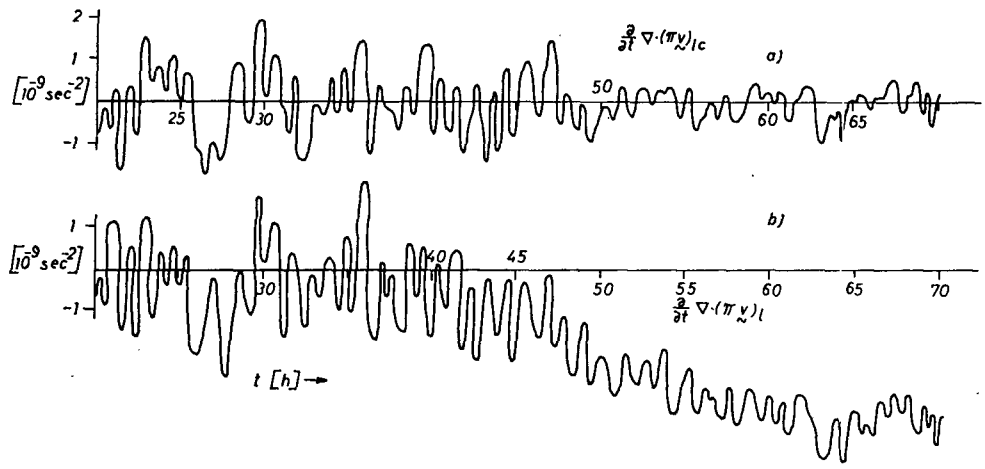

FIG. 9. Long barrier. Grid point (12; 12). The tendency of the divergence in the lowest layer computed with (a) and without (b) corrections for the influence of the wall.

ture in the layer $1 \geq \sigma \geq 0.5$ compared with the environment. The deviation (T_m') from the temperature T_m in the middle layer from the initial value is shown in Fig. 7(c). Waves of relatively warm air are registered until $t = 36$ hr, followed by a monotonic increase of T_m' until 55 hr. Cooling is seen later on. These changes of the temperature can be explained as follows.

Figure 8 shows the deviation of the temperature from the basic initial state in $\sigma = 0.7$ after 48 hr. Warm air is moving northeastward in front of the trough and the highest temperatures are seen above the area of greatest pressure fall. The penetration of warm air in front of the parent upper level trough into the region of strongest development is also clearly seen in the charts of Bonner (1961), McClain (1960), Newton (1956), and Carlson (1961). Later on, cold air is protruding towards the lee (see Fig. 4) and causes the temperature fall.

Let us now turn to a discussion of the influence of the lee wall on the development. The quantity $\partial/(\partial t)\nabla\cdot(\pi\mathbf{V})_i$ should be calculated by use of the corrected terms $-\nabla\cdot(RT\nabla\pi)_{ic}$ and $-\nabla\cdot(\pi\nabla\Phi)_c$ in (3), as mentioned above. The result is displayed in Fig. 9(a). The oscillations of $\partial/(\partial t)\nabla\cdot(\pi\mathbf{V})_{ic}$ result in corresponding variations of $\nabla\cdot(\pi\mathbf{V})_i$ (Fig. 7b). It is interesting to compare Fig. 9(a) to Fig. 9(b) where that tendency of $\nabla\cdot(\pi\mathbf{V})_i$ is shown which would result at each time step if the wall were removed at each time step; i.e., Fig. 9(b) is calculated without corrections of $-\nabla\cdot(RT\nabla\pi)$ and $-\nabla\cdot(\pi\nabla\Phi)$ in (12; 12). The quantity $\partial/(\partial t)\nabla\cdot(\pi\mathbf{V})_{ic} > \partial/(\partial t)\nabla\cdot(\pi\mathbf{V})_i$ almost all the time until 40 hr. There is a pronounced tendency towards convergence ($\nabla\cdot(\pi\mathbf{V})_i < 0$) later on. The wall hinders any inflow from the west, which would set in immediately after the wall's removal—at least after 40 hr. Thus, the new center of low pressure is protected by the wall. Divergence can be maintained in the lowest level even long after the beginning of the pressure fall.

Summing up, we can state that our experiment simulated fairly realistically a case of weak cyclogenesis in the lee of the Rocky Mountains. The penetration of warm air above the mountains that stems from the warm sector of the parent cyclone results in a tendency towards divergence, in the upper levels above the lee wall, which creates a pressure fall. The new center of low pressure is protected by the mountains from being filled by low-level convergence. The pressure fall is terminated by the protrusion of cold air across the barrier. Vorticity advection has no significant influence on the low-level development.

5. Barrier of 2400 km length—Greenland

The second experiment reported on in this paper is concerned with a north-south barrier of 2400 km length and 2000 m height, as shown in Fig. 1. Greenland with its length of about 2500 km and a height between 2000 m and 3000 m is depicted in a crude fashion by this barrier. Nevertheless, it has been shown (Egger, 1972a), that our model is able to produce flow patterns near the barrier that are similar to observed ones in the Greenland area.

Lee cyclogenesis near the southern tip of Greenland is often observed when a low is approaching the central or southern part of Greenland from the west (Walden, 1959). Therefore, it seems to be reasonable to use a similar initial situation in the Greenland case as in the previous experiment: a low, moving towards the barrier in a straight baroclinic current. The low in the Greenland case has an initial position in the channel which is about 1000 km south of that in the Rocky Mountains case. Otherwise, the initial fields are identical. In the Rocky Mountains case, almost no air could go around the barrier in the lowest level and influence the lee side development. Now, the barrier is shorter and it might

be interesting to compare the developments in both cases.

Figure 10 shows the deviation of the surface pressure from the basic initial state after 60 hr. The surface low moved straight towards the barrier during the first day (dots), decelerated, curved towards the north, and disappeared. The pressure fall begins along the east coast at about $t=30$ hr and strong cyclonic activity is seen with its center to the south of the track of the parent cyclone. This center is about to move northeastward at $t=60$ hr. There is cyclonic flow around the southern tip of the barrier. Weak northerly flow is seen along the east coast after southerly flow had prevailed during most of the development. A "cold front" is crossing the barrier in $\sigma=0.7$ and is passing by the southern tip in the lowest level. The upper trough is crossing the barrier at $t=60$ hr. Its center is now recurving towards the north and will take over the new surface center one day later (Fig. 11).

Such a pattern is frequently observed: a low approaches the central part of Greenland from the west or southwest. After the center arrives at the west coast, pressure begins to rise. The center remains at the west coast, sometimes moving towards the north, and fills up. In the mean time, a new development occurs near the southern tip of Greenland, at times as much as 1000 km south of the parent center. It is often observed that the pressure fall east of Greenland is more intense than that on the west coast, which is connected with the primary cyclone. Initially, the new center is almost stationary, but moves towards the east or northeast after it becomes associated with the center aloft (Dorsey, 1945; Rodewald, 1955; Putnins, 1970; see in particular Fig. 11 by Walden, 1955).

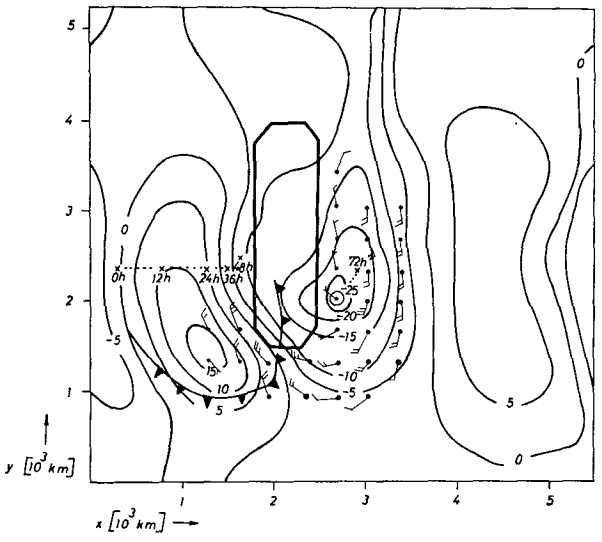

FIG. 10. The 2400-km barrier. Deviation of the surface pressure (mb) from the basic initial state after 60 hr. Wind in $\sigma=0.9$ (odd time step). Track of the center of the low (dots). Grid point (12; 12) encircled.

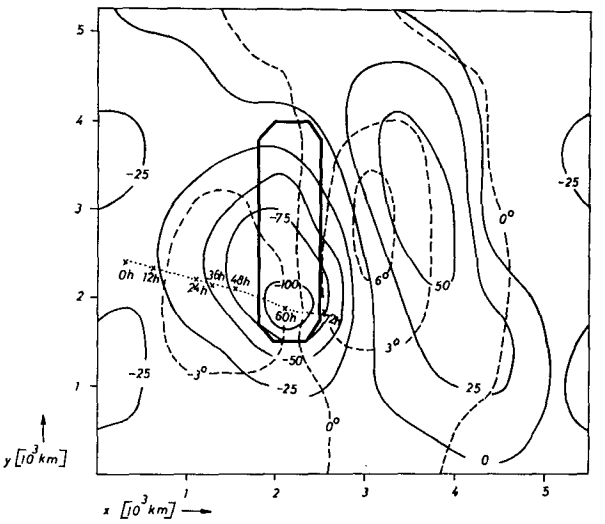

FIG. 11. The 2400-km barrier; $t=60$ hr. Deviation of the 500-mb surface (m) from the basic initial state (solid). Deviation of the temperature (°C) in $\sigma=0.7$ (dashed). Track of the center of the low at 500 mb.

Unfortunately, the investigators of the behavior of the lows near Greenland made no attempt to assess the influence of the vorticity aloft, of the temperature field, etc., on the development—with the exception of a paper of Wishman (1971), who analyzed a case that is quite different from ours.

Figure 12 is analogous to Fig. 7. Again the point of greatest pressure fall has been chosen, which is the grid point (12; 8) at $t=60$ hr (circle in Fig. 10). The pressure fall commences when the surface center has reached the west coast (30 hr) and amounts to 25 mb at the end of the development. The quantity $-\nabla^2\pi$ reaches its minimum before the end of the pressure fall and rises later on, thus indicating a spreading and a movement of the new cyclone towards the east. We have always $-\nabla^2\pi_c > -\nabla^2\pi$. A positive sign of $\nabla\cdot(\pi\mathbf{V})$ prevails in the upper and lowest layer all the time, convergence in the middle layer. Therefore, the flow in the upper layer must be responsible for the initiation of the pressure fall and is supported by the divergence in the lowest layer later on. The quantity $-\nabla\cdot(\pi\nabla\Phi)$ is cyclogenetic all the time. The pressure fall begins with the rise of $-\nabla\cdot(\pi\nabla\Phi)_u$ at $t=31$ hr. The temperature field in the upper layer does not contribute significantly to $-\nabla\cdot(\pi\nabla\Phi)_u$ at the beginning of the development; $-\nabla\cdot(\pi\nabla\Phi)_{lc}$ is unimportant.

Vorticity is the other factor that could cause an increase of $\nabla\cdot(\pi\mathbf{V})$ and a pressure fall. We notice a steady increase of CVORT_l. Therefore, the divergence in the lowest layer seems to be created by the vorticity. That is not the case in the other layers, for there the vorticity attains to positive values long after the low-level development has begun. The role of DHA can be seen in Fig. 13(a); note that the vertical scale is increased by a factor 10 compared with Fig. 12(c,d).

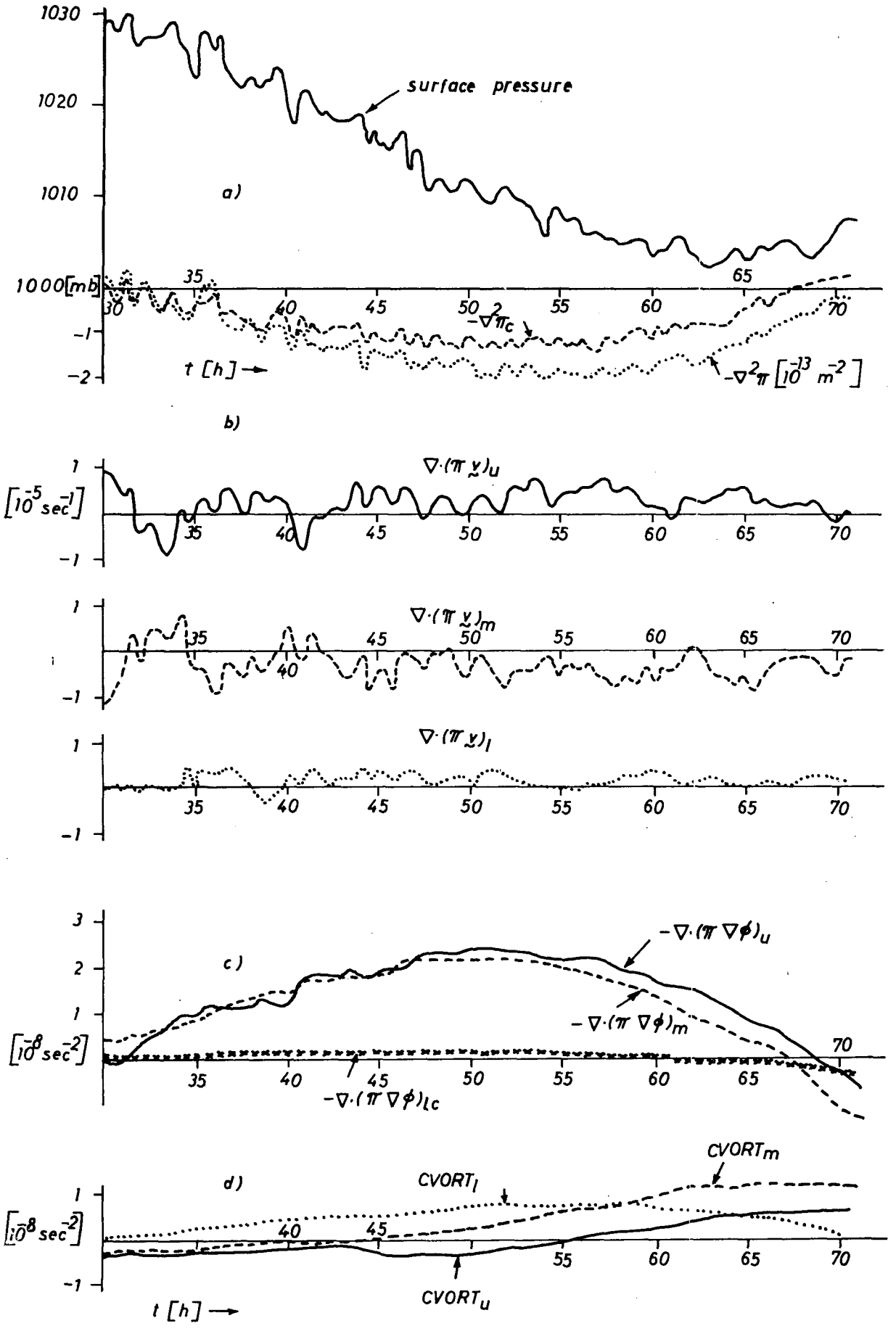

FIG. 12. The 2400-km barrier. Grid point (12; 8); $30 \leq t \leq 70$ hr, Legend see Fig. 7.

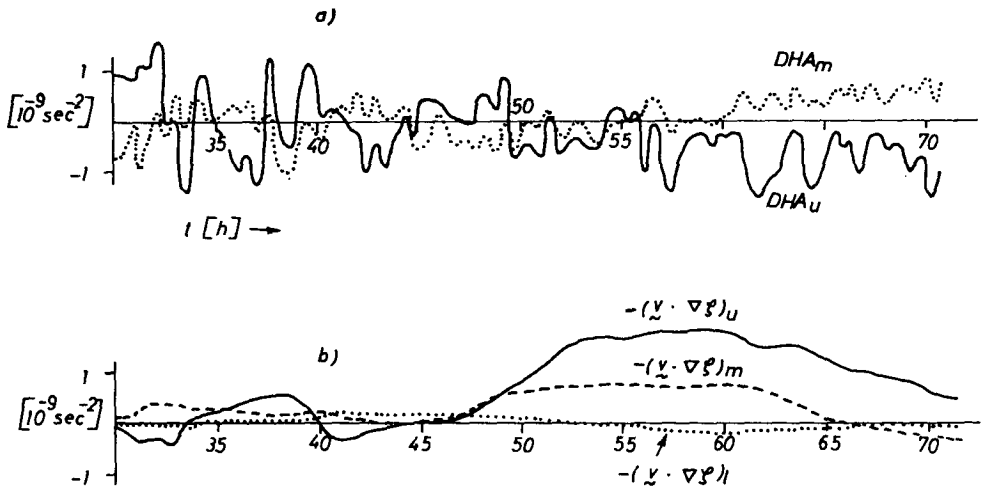

FIG. 13. The 2400-km barrier. Grid point (12; 8). (a) DHA in the middle and upper layer. (b) Vorticity advection in all layers.

DHA seems to have no cyclogenetic influence in the middle and upper layer until $t=50$ hr. DHA$_u$ produces convergence, DHA$_m$ divergence later on.

It can be concluded that the cyclogenesis is initiated and maintained by an increase of $-\nabla\cdot(\pi\nabla\Phi)$ in the middle and upper layer. Divergence and descent in the lowest layer support the development. Vorticity comes into play in the middle and upper layer about one day after the beginning of the pressure fall.

As in the Rocky Mountains case, we have to explain the increase of $-\nabla\cdot(\pi\nabla\Phi)_{m,u}$ at about $t=30$ hr. The key to this question is contained in Fig. 11. We observe —as in Fig. 8—a broad area of warm air with $-\nabla^2T>0$ moving in front of the trough across the cyclogenetic region. Cold air is approaching the east coast, which causes a decrease of $-\nabla\cdot(\pi\nabla\Phi)_{m,u}$ after $t=55$ hr, Fig. 12(c). The temperature field in $\sigma=0.5$ is very similar to that shown in Fig. 11 but has only half the intensity. The low-level development is initiated by the thermal field of the upper trough that is crossing the mountain.

The influence of the wall on the thermal field can be studied by performing an experiment without the barrier, starting from the same initial situation as in the Greenland case. This time, the low is moving straight towards the east and the pressure fall in (12; 8) amounts to 30 mb at $t=60$ hr. We observe $\nabla\cdot(\pi\mathbf{V})>0$ in the upper layer, $\nabla\cdot(\pi\mathbf{V})<0$ in the lowest layer during the period of development at (12; 8), whereas the sign of $\nabla\cdot(\pi\mathbf{V})_m$ is often changing; $-\nabla\cdot(\pi\nabla\Phi)_m$ is rising at $t=40$ hr and reaches a maximum value of 1.2 10^{-8} s^{-2} at 60 hr, considerably less than in the Greenland case.

Figure 14 shows the surface pressure after 60 hr in the experiment without mountains. The low moved towards the east and deepened. The central pressure is 10 mb below that of the lee low in Fig. 10. Nevertheless, the similarity of Fig. 14 and Fig. 10 is striking. The mountain blocks the low pressure system near the surface but the upper part of this system crosses the mountain and establishes a new center of cyclonic vorticity in the lowest level almost at the same place as in the case without the mountain. Such a process should perhaps be called the crossing of a mountain barrier by a low pressure system and not lee cyclogenesis.

Figure 15(a) shows the deviation $T_{m,l}'$ of $T_{m,l}$ from the initial value in both experiments. The advection of warm air in front of the approaching low effects a steady increase of T_l' in the experiment without the barrier. The mountain does not seem to hinder this advection—T_l' is rising in the Greenland case as if there were no barrier. On the other hand, the pro-

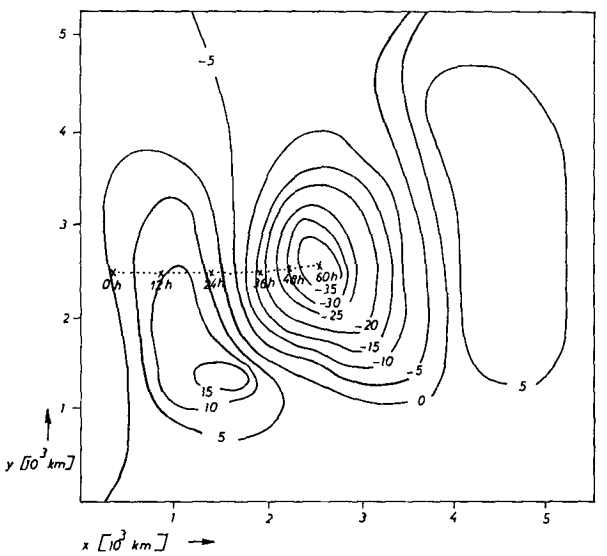

FIG. 14. Experiment without barrier. Deviation of the surface pressure (mb) from the initial basic state after 60 hr. Dots: track of the low's center.

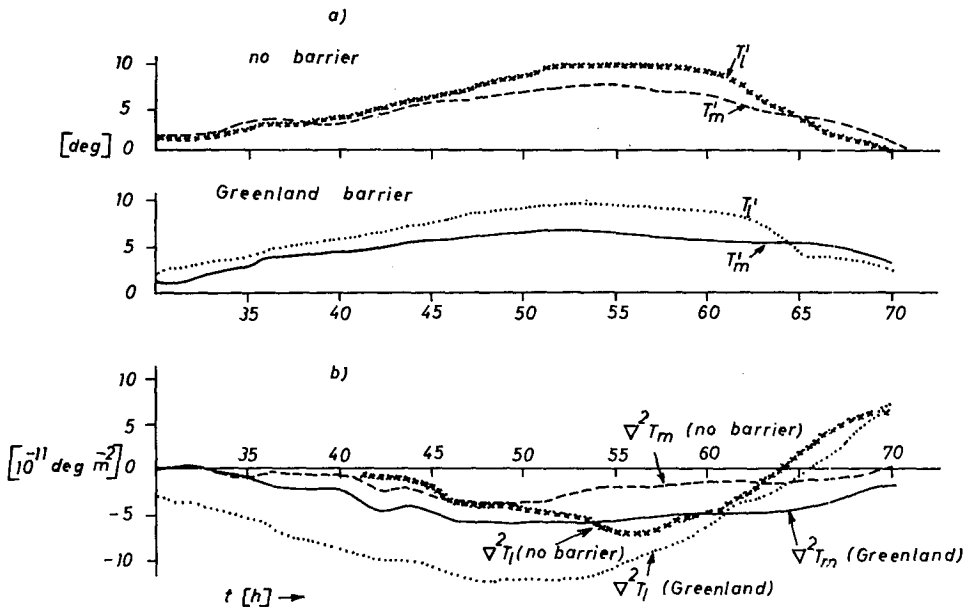

FIG. 15. Grid point (12; 8). Deviation T_m', T_l' of T_m, T_l from the initial state and $\nabla^2 T_l$, $\nabla^2 T_m$ in the Greenland case and in the experiment without a barrier.

trusion of cold air towards the east is hampered by the mountain. The air in the middle layer is slightly cooler than in the Greenland case, but the trend is almost the same in both experiments.

One could rather be inclined to assume that the course of $\nabla^2 T$ is also very similar in both experiments. However, it can be seen from Fig. 15(b) that $\nabla^2 T_l$ is considerably less in the Greenland case than in the run without the barrier. The same is true for $\nabla^2 T_m$, but to a lesser extent. It is easy to explain the difference in the lowest layer. The temperature rises in all grid points near (12; 8) in the experiment without a barrier and, therefore, $\nabla^2 T_l$ falls only slowly in (12; 8). On the other hand, there is no warming in (11; 8) in the lowest level in the Greenland case. Therefore, any warming in (12; 8) results in a more intense decrease of $\nabla^2 T_l$. This decrease does not contribute to a rise of $-\nabla\cdot(\pi\nabla\Phi)$ in the lowest level in (3), for there a corrected form of $-\nabla\cdot(\pi\nabla\Phi)$ has to be used which disregards T in (11; 8). The quantity $\nabla^2 T_l$ is taken fully into account in the vertical integral (7) for the middle layer. Therefore, $-\nabla\cdot(\pi\nabla\Phi)$ is much greater in (12; 8) in the Greenland case than in the other experiment and the thermal field has a more pronounced cyclogenetic effect which is caused by the barrier. This effect is considerably increased by the fact that also $\nabla^2 T_m$ is less in the Greenland case. The reasons for these low values of $\nabla^2 T_m$ are not clear. The advection of warm air above the barrier in (11; 8) is perhaps not as intense as in the experiment without mountains. It can be stated that the mountain wall acts toward an increase of the cyclogenetic effect of the advective warming in front of the parent low. This increase is necessary to set off the anticyclonic influence of the distribution of the surface pressure, which is much greater in the Greenland case than in the other experiment because of the small horizontal extension of the pressure fall area.

Turning to a discussion of the influence of the vorticity on the pressure fall, we have to look for the advection of vorticity, Fig. 13(b). There is almost no vorticity advection until 48 hr and a relatively sharp increase later on except in the lowest layer. The growth of $-\mathbf{V}\cdot\nabla\zeta_{m,u}$ is connected with the approach of the trough from the west (Fig. 11). Hence, the increase of $\mathrm{CVORT}_{m,u}$ in Fig. 12 is mainly effected by the advection of vorticity, whereas the positive vorticity in the lowest layer is created by low-level divergence.

Summing up, we can state that the pressure fall in the grid point (12; 8) is initiated by divergence $(\nabla\cdot(\pi\mathbf{V})>0)$ aloft caused by the approach of warm air above the barrier in front of the parent trough. The pressure fall causes southerly flow along the east coast, which warms the lowest layer. This low-level warming increases significantly the cyclogenetic influence of $-\nabla\cdot(\pi\nabla\Phi)$ in the middle and upper layer. These cyclogenetic factors are partly counterbalanced by $-\nabla\cdot(RT\nabla\pi)$, which attains large values because of the small horizontal extension of the area of pressure fall. Vorticity advection has no influence during the first stage of development; it strengthens the new cyclone after it has been formed. The development is terminated by the approach of the cold front above the barrier and around the southern tip of Greenland.

The numerical experiments and their comparison with observed cases have shown that the mechanism

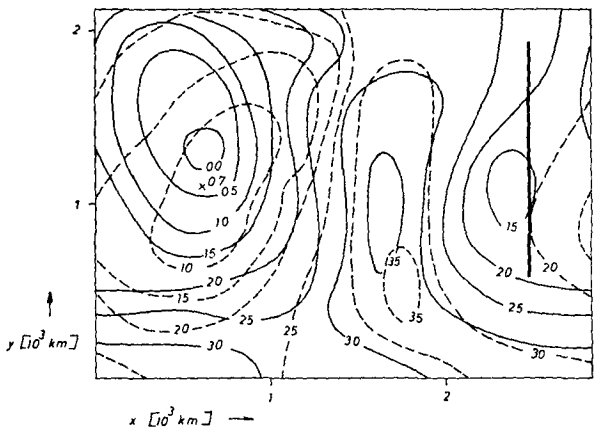

FIG. 16. Surface pressure (mb) after 72 hr in the fine-mesh experiment ($Dx=175$ km; solid) and in the coarse mesh run ($Dx=350$ km; dashed). The mountain wall is given by the heavy solid line. Cross: center of the low in the coarse mesh run.

of lee cyclogenesis is almost the same on the eastern wall of the long barrier and near the southern tip of the Greenland barrier. The development near the southern tip is more intense than in the lee of the long barrier. This difference might be caused by the ridge east of the barrier, which is more intense during the first experiment—presumably due to the influence of the northern wall of the channel—and by the strong flow around the southern tip of the barrier in the Greenland case which is almost absent during the first experiment.

6. Discussion

Our analysis and explanation of the lee cyclogenesis depend to some extent on the design of the experiments and on the numerical structure of the model. It is conceivable that small changes in the initial conditions or an increase of the horizontal and/or vertical resolution of the model would result in quite different flow patterns. A series of experiments has been carried out in which the intensity and the size of the low to the west of the barrier have been changed. Furthermore, a basic flow with horizontal shear has been used. Of course, these changes influenced the intensity and the course of the lee cyclogenesis. But the basic mechanism was the same in all experiments, i.e., the pressure fall in the lee is caused by a sharp increase of $-\nabla\cdot(\pi\nabla\Phi)$ in the middle layer. A significant contribution of the vorticity to the pressure fall has not been observed. In all experiments, the basic current initially satisfied the boundary condition (1) at the barrier in $\sigma=0.9$. Otherwise, the mountain would perturb the basic flow and these perturbations could result in developments of highs and lows that would considerably complicate the discussion of the flow patterns.

The influence of the resolution of the model on the cyclogenetic process could be tested by doubling the number of grid points in the channel. Unfortunately, lack of computer facilities prevented such an experiment. Instead, we have tested the influence of the horizontal resolution by running two experiments in a channel of only 1950 km width and 2800 km length and with three layers in the vertical. We have the same low as in the previous experiments and a zonal flow $\bar{u}=40(1-\sigma)-6.7$ m s^{-1} at the beginning of the experiments. The low drifts in the basic current towards a simple wall which blocks the flow in the lowest layer over a distance of 1400 km (heavy solid line in Fig. 16). The first experiment is made with a grid length $Dx=350$ km, the second one with $Dx=175$ km. The results are compared in Fig. 16.

In both experiments, the pressure fall begins in the lee at about $t=36$ hr. The new center is fully developed at about 60 hr and drifts towards the east later on. After 72 hr, the new low in the fine mesh run (solid) is more intense than in the coarse mesh case (dashed). We notice a remnant of the parent low in the fine mesh run which has disappeared in the coarse mesh experiment. In general, however, the coarse mesh predictions are rather close to those of the fine mesh run. Therefore, it is reasonable to assume that a refinement of the horizontal resolution would not have basically changed the flow patterns in the Greenland experiment or in the Rocky Mountains case.

Our study of the mechanism of lee cyclogenesis is based on the discussion of the terms of the vorticity and the divergence equation in one grid point. It is conceivable that the same procedure would yield quite different results when applied in an adjacent grid point. Figure 17 shows the average value of the main terms of the divergence equation for the grid points (12; 8), (13; 8), (12; 7), (13; 7) in the Greenland experiment. It is seen that the term $-\nabla\cdot(\pi\nabla\Phi)$ initiates the pressure fall just as in Fig. 12. CVORT is

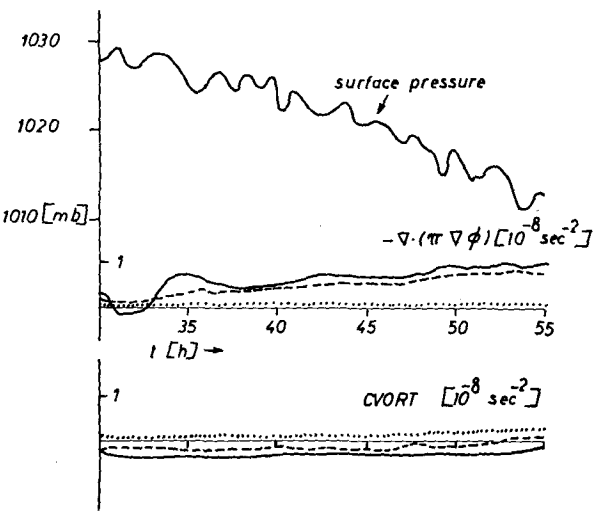

FIG. 17. Average value of the surface pressure, $-\nabla\cdot(\pi\nabla\Phi)$ and CVORT in the grid points (12; 8), (12; 7), (13; 8), (13; 7) in the Greenland experiment.

negative in the upper and middle layer and does not contribute to the pressure fall. The amplitude of $-\nabla\cdot(\pi\nabla\Phi)$ is reduced, compared to Fig. 12, but the shape of the curves is quite similar. We conclude that the results of the analysis in the point (12; 8) are representative for all grid points in the area of the most intense pressure fall.

The application of the boundary condition (1) in a model with a staggered grid may result in a tendency towards a separation of the forecasts at even and odd time steps (Egger, 1972a). In order to counteract this effect we use a rather large horizontal momentum diffusion coefficient in the prognostic equations of the model, neglected in (4), (5), (10), (11),

$$u_t = \cdots + A(\overset{-xy}{u}^{(n)} - u^{(n-1)}),$$

with $A = 3/48h^{-1}$; n is the index of the time steps. The diffusive terms connects the values of u at even and odd time steps and effectively reduces the separation of the forecasts (Edelmann, 1963).

Acknowledgment. The author is grateful to the reviewers for suggesting several improvements.

REFERENCES

Bonner, W. D., 1961: Development processes associated with the formation and movement of an Alberta cyclone. University of Chicago, Tech. Rep. No. 4, Contr. Nr. 2121(10), NR 082 161.

Carlson, T. N., 1961: Lee-side frontogenesis in the Rocky Mountains. *Mon. Wea. Rev.*, **89**, 163–172.

Dorsey, H. G., 1945: Some meteorological aspects of the Greenland ice cap. *J. Meteor.* **2**, 135–142.

Edelmann, W., 1963: On the behaviour of disturbances in a baroclinic channel. Res. Div. German Weath. Serv., Tech. Note 7.

Egger, J., 1972a: Incorporation of steep mountains into numerical forecasting models. *Tellus*, **24**, 324–335.

——, 1972b: Numerical experiments on the cyclogenesis in the gulf of Genoa. *Beitr. Phys. Atmos.*, **45**, 320–346.

Hage, K. D., 1961: On summer cyclogenesis in the lee of the Rocky Mountains. *Bull. Amer. Meteor. Soc.*, **42**, 20–33.

Hess, S. L., and H. Wagner, 1948: Atmospheric waves in the northwestern United States. *J. Meteor.* **5**, 1–19.

Klein, W. H., 1957: Principal tracks and mean frequencies of cyclones and anticyclones in the northern hemisphere. *U. S. Weather Bureau Research Paper 40.*

McClain, E. P., 1960: Some effects of the western Cordillera if North America on cyclone activity. *J. Meteor.* **17**, 104–115.

Newton, C. W., 1956: Mechanisms of circulation change during a lee cyclogenesis. *J. Meteor.*, **13**, 528–539.

Putnins, P., 1970: The climate of Greenland. *World Survey of Climatology. Climate of the Polar Regions.* Elsevier, 3–109.

Rodewald, M., 1955: Klima und Wetter der Fischereigebeit West-und Südgrönland. Deutscher Wetterdienst, Seewetteramt.

Walden, H., 1959: Statistisch-synoptische Untersuchungen über das Verhalten von Tiefdruckgebieten im Bereich von Grönland. Deutscher Wetterdienst, Seewetteramt.

Wishman, E. H., 1971: On a cyclone development off northeast Greenland. *Met. Annaler*, **6**.